LETTER

doi:10.1038/nature17974

Single-molecule strong coupling at room temperature in plasmonic nanocavities

Rohit Chikkaraddy[1], Bart de Nijs[1], Felix Benz[1], Steven J. Barrow[2], Oren A. Scherman[2], Edina Rosta[3], Angela Demetriadou[4], Peter Fox[4], Ortwin Hess[4] & Jeremy J. Baumberg[1]

Photon emitters placed in an optical cavity experience an environment that changes how they are coupled to the surrounding light field. In the weak-coupling regime, the extraction of light from the emitter is enhanced. But more profound effects emerge when single-emitter strong coupling occurs: mixed states are produced that are part light, part matter[1,2], forming building blocks for quantum information systems and for ultralow-power switches and lasers[3–6]. Such cavity quantum electrodynamics has until now been the preserve of low temperatures and complicated fabrication methods, compromising its use[5,7,8]. Here, by scaling the cavity volume to less than 40 cubic nanometres and using host–guest chemistry to align one to ten protectively isolated methylene-blue molecules, we reach the strong-coupling regime at room temperature and in ambient conditions. Dispersion curves from more than 50 such plasmonic nanocavities display characteristic light–matter mixing, with Rabi frequencies of 300 millielectronvolts for ten methylene-blue molecules, decreasing to 90 millielectronvolts for single molecules—matching quantitative models. Statistical analysis of vibrational spectroscopy time series and dark-field scattering spectra provides evidence of single-molecule strong coupling. This dressing of molecules with light can modify photochemistry, opening up the exploration of complex natural processes such as photosynthesis[9] and the possibility of manipulating chemical bonds[10].

Creating strongly coupled mixed states from visible light and individual emitters is severely compromised by the hundred-fold difference in their spatial localization. To overcome this, high-quality cavities are used to boost interaction times and enhance coupling strengths. However, in larger cavities the longer round trip for photons to return to the same emitter decreases the coupling, which scales as $g \propto 1/\sqrt{V}$, where V is the effective cavity volume and g is the coupling energy. This coupling has to exceed both the cavity loss rate, κ, and the emitter scattering rate, γ, in order for energy to cycle back and forth between matter and light components, requiring $2g > \gamma, \kappa$ (ref. 11). For cryogenic emitters[5,6] (laser-cooled atoms, vacancies in diamond, or semiconductor quantum dots), the suppressed emitter scattering allows large cavities (with a high quality factor, Q, which is proportional to κ^{-1}) to reach strong coupling. Severe technical challenges, however, restrict the energy, bandwidth, size and complexity of devices. Progress towards room-temperature devices has been limited by the unavoidable increase in emitter scattering, and the difficulty of reducing the volume of dielectric-based microcavities—at wavelength λ and refractive index n—below $V_\lambda = (\lambda/n)^3$. At room temperature, typical scattering rates for embedded dipoles are $\gamma \sim k_B T$, implying that suitable $Q < 100$, which thus requires cavities of less than $10^{-5} V_\lambda$ (Fig. 1a, dark green shaded area).

Improved confinement uses surface plasmons (Fig. 1a), combining oscillations of free electrons in metals with electromagnetic waves[12]. Structured metal films can couple molecular aggregates of high oscillator strength, but far too many molecules are involved for quantum optics. Recent studies have reached 1,000 molecules[13–15]—still far above the one to ten molecules that are needed to access quantum effects at room temperature.

To create such small nanocavities and orient single molecules precisely within them, we use bottom-up nanoassembly. Although field volumes of individual plasmonic nanostructures are too large[1,2], smaller volumes and stronger field enhancements occur within subnanometre gaps between paired plasmonic nanoparticles. We use the promising nanoparticle-on-mirror (NPoM) geometry[16], placing emitters in the gap between nanoparticles and a mirror underneath (Fig. 1b). This gap is accurately controlled to a subnanometre scale using molecular spacers, is easily made by depositing monodisperse metal nanoparticles onto a metal film, and is scalable, repeatable and straightforward to characterize[17,18]. Specifically, we use gold nanoparticles of 40-nm diameter on a 70-nm-thick gold film, separated by a 0.9-nm molecular spacer (see below). The intense interaction between each nanoparticle and its image forms a dimer-like construct with field enhancements of $\sim 10^3$, and an ultralow mode volume. The coupled plasmonic dipolar mode is localized in the gap (Fig. 1b), with the electric field oriented vertically (along the z direction). The resonant wavelength is determined by the nanoparticle size and gap thickness, and can thus be tuned from 600 nm to 1,200 nm (ref. 17).

Several factors are essential in positioning a quantum emitter inside these small gaps. One is to prevent molecular aggregation, which occurs commonly. Another is to ensure that the transition dipole moment, $\boldsymbol{\mu}_m$, is perfectly aligned with the gap plasmon (along the electric field). We use a common dye molecule, methylene blue, with a molecular transition at 665 nm, to which our plasmons are tuned. To avoid aggregation of the dye molecules and to assemble them in the proper orientation, we use the host–guest chemistry of macrocyclic cucurbit[n]uril molecules. These are pumpkin-shaped molecules with varying hollow hydrophobic internal volumes, determined by the number of units in the ring (n), in which guest molecules can sit (Supplementary Fig. 1)[19]. Cucurbit[7]uril is water-soluble and can accommodate only one methylene-blue molecule inside. Encapsulation of methylene blue inside cucurbit[7]uril is confirmed by absorption spectroscopy (Fig. 2a): methylene-blue dimers (shown by the small 'shoulder' peak at 625 nm on the red curve) disappear on mixing low methylene-blue concentrations with cucurbit[7]uril (in a 1:10 molar ratio) (Fig. 2a, blue curve). Control experiments with the smaller cucurbit[5]uril molecules (into which methylene blue cannot fit) do not remove this shoulder peak (Fig. 2a, dashed line), ruling out parasitic binding. Placing single methylene-blue molecules into cucurbit[7]uril thus avoids any aggregation. Carbonyl portals at either end of the 0.9-nm-high cucurbit[n]uril molecules bind them with their rims flat onto the gold surface (Fig. 2b). When a monolayer of cucurbit[7]uril is first deposited on the gold mirror and suitably filled with methylene-blue molecules, gold nanoparticles can bind on top to form the desired filled nanocavity

[1]NanoPhotonics Centre, Cavendish Laboratory, University of Cambridge, Cambridge CB3 0HE, UK. [2]Melville Laboratory for Polymer Synthesis, Department of Chemistry, University of Cambridge, Lensfield Road, Cambridge CB2 1EW, UK. [3]Department of Chemistry, King's College London, London SE1 1DB, UK. [4]Blackett Laboratory, Department of Physics, Prince Consort Road, Imperial College, London SW7 2AZ, UK.

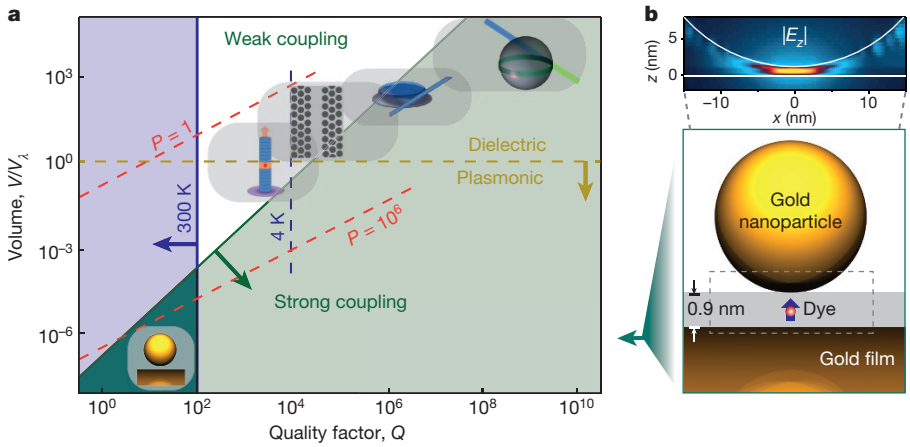

Figure 1 | Comparing single-molecule optical cavities. a, The quality factor, Q, of a nanocavity is plotted against its effective volume, V/V_λ (scaled to $V_\lambda = (\lambda/n)^3$), showing strong-coupling (green arrow), room-temperature (blue arrow), and plasmonic (orange arrow) regimes for single emitters. The icons show realizations of each type of nanocavity: from right, whispering gallery spheres (used as microresonators in filters, sensors and lasers), microdisks, photonic crystals (with possible applications in optical computing), micropillars (used in high-throughput screening), and nanoparticle-on-mirror geometry (NPoM, used here). Purcell factors (P) show emission-rate enhancements. **b**, Diagram of a NPoM. The blue arrow in the gap between the nanoparticle and the mirror locates the transition dipole moment of the emitter. The inset above shows the simulated near-field of the coupled gap plasmon in the dashed box, with maximum electric field enhancement of about 400, oriented vertically (in the z direction).

(Fig. 2b and Supplementary Information), with the methylene-blue molecule aligned vertically in the gap[19]. Previous studies[17] with empty cucurbit[n]urils show that the gap is 0.9 nm, with a refractive index of 1.4.

Dark-field scattering spectra from individual NPoMs show the effect of aligning the emitter in different orientations (Fig. 3a). With $\boldsymbol{\mu}_m$ parallel to the mirror (top; without cucurbit[n]urils the methylene blue lies flat on the metal surface), the resonant scattering plasmonic peak (ω_p) is identical to that of NPoMs without any emitters (ω_0). But with $\boldsymbol{\mu}_m$ perpendicular to the mirror (bottom), the spectra show two split peaks (ω_+ and ω_-) resulting from the strong interaction between emitters and plasmon. We contrast three types of samples. Without dye (Fig. 3b, top), a consistent gap plasmon (ω_p) at 660 ± 10 nm is seen. Small fluctuations in peak wavelength are associated with $\pm$5-nm variations in nanoparticle size (Supplementary Fig. 2). When this NPoM is partially filled with methylene blue inside the cucurbit[7]uril, peaks at 610 nm and 750 nm are seen either side of the absorption peak of methylene blue at ω_0 (Fig. 3b, bottom), corresponding to the formation of hybrid plasmon–exciton ('plexciton') branches, $\omega_\pm = \omega_0 \pm g/2$. This yields a Rabi frequency of $g = 380$ meV, confirmed by full three-dimensional finite-difference time-domain (FDTD) simulations (Supplementary Fig. 3). While some studies[13,14] have shown significant variations in $\omega_\pm$, we obtain highly consistent results, with no spectral wandering observed on individual NPoMs. With dye molecules perpendicular to the plasmon field (without cucurbit[n]urils), only a gap plasmon is seen (Supplementary Fig. 4c). Methylene-blue molecules self-assembling on gold orient flat to the surface, owing to π-stacking interactions between the conjugated phenyl rings and the metal film[20]. Our study thus shows how molecular scaffolding is essential to yield molecular coupling to the gap plasmon.

To map the dispersion curve, we combine scattering spectra from differently sized nanoparticles, plotted according to their detuning from the absorption ('exciton') resonance. Simulations of nanoparticles of 40–60 nm in diameter (Supplementary Fig. 5) show gap plasmons tuning across the exciton. A simple coupled-oscillator model matches the quantum mechanical Jaynes–Cummings picture[13]:

$$\omega_\pm = \frac{1}{2}(\omega_p + \omega_0) \pm \frac{1}{2}\sqrt{g^2 + \delta^2}$$

with plasmon and exciton resonance energies ω_p and ω_0, and detuning energies of $\delta = \omega_p - \omega_0$. Extracting $\omega_\pm$ from the scattering spectra allows ω_p to be calculated (knowing ω_0, which does not show any spectral wandering). This fitting reveals typical anticrossing (mixing) behaviour (Fig. 3c), with $g = 305 \pm 8$ meV at $\delta = 0$. We find $2g/\gamma_{pl} \sim 5$, well into the strong coupling regime. A key figure of merit is the Purcell factor, $P = Q/V$, which characterizes different cavity systems (Fig. 1a). For our plasmonic nanocavities, $P \approx 3.5 \times 10^6$ (Supplementary Fig. 6); this is over an order of magnitude larger than the Purcell factors of state-of-the-art photonic crystal cavities[5], which have reached 10^5, while state-of-the-art planar micropillars[21,22] attain Purcell factors of 3×10^5. The ultralow cavity volume arises here because of the very large field confinement in such nanometre-sized gaps (Supplementary Fig. 9e). Such Purcell factors imply photon emission times below 100 femtoseconds, seen as the $\hbar/g \sim$30-femtosecond Rabi flopping, but very short to measure directly.

To probe single-molecule strong coupling, we systematically decrease the number of methylene-blue molecules by reducing the ratio of methylene blue to cucurbit[7]uril. Previous studies and simple area estimates imply that 100 cucurbit[7]uril molecules lie inside each nanocavity (Supplementary Fig. 9). With the initial 1:10 molar ratio of methylene

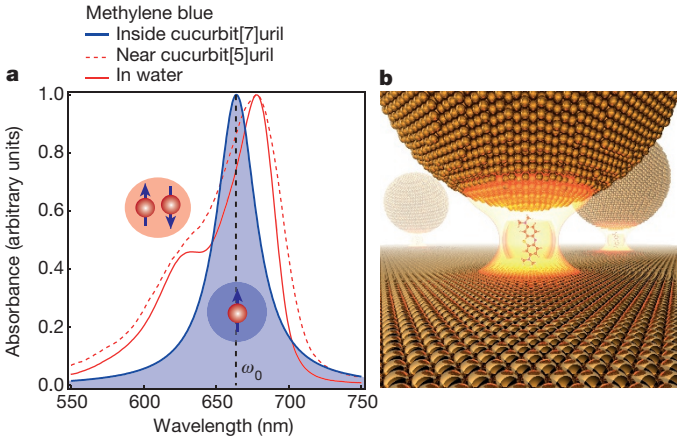

Figure 2 | Plasmonic nanocavity containing a dye molecule. **a**, Absorption spectra of methylene blue in water, with (blue) and without (red) encapsulation in cucurbit[n]urils of different diameters (dashed and solid red lines). Icons show individual molecules (in blue; line centred at ω_0) and paired molecular dimers (in red). **b**, Illustration of a methylene-blue molecule in cucurbit[n]uril, in the nanoparticle-on-mirror geometry used here.

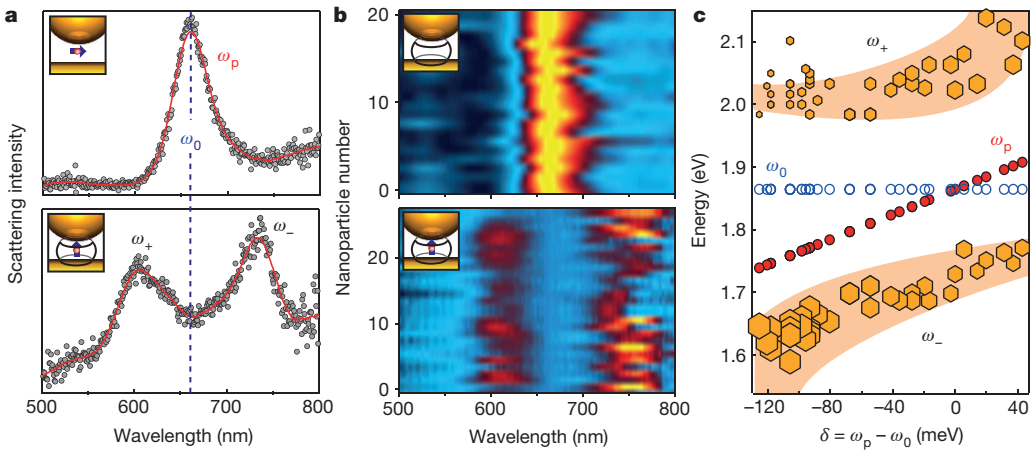

Figure 3 | Strong coupling seen in scattering spectra of individual NPoMs. a, Scattering spectra resulting from isolated NPoMs according to the orientation of the emitter (the methylene-blue dye; see insets). With the dye transition dipole moment, $\boldsymbol{\mu}_m$, oriented parallel to the mirror, the resonant scattering plasmonic peak (ω_p) is identical to that of NPoMs without any emitters. With $\boldsymbol{\mu}_m$ oriented parallel to the mirror, split peaks result from the strong interaction between the emitter and the plasmon. The blue dashed line indicates the dye's absorption wavelength (centred at ω_0). **b**, Comparison of scattering spectra from different NPoMs (see insets), whose gaps are filled by a cucurbit[7]uril monolayer that is empty (top), or encapsulating dye molecules (bottom). **c**, Resonant positions of methylene-blue (ω_0), plasmon (ω_p) and hybrid modes (ω_+ and ω_-) as a function of extracted detuning. The symbol size depicts the amplitude in scattering spectra.

blue:cucurbit[7]uril, the mean number ($\bar{n}$) of methylene-blue molecules within each mode volume is thus 10. We explore many plasmonic nanocavities with a mean dye number of 10 or less (Fig. 4a). From the resulting spectra, we extract coupling strengths at different mean dye numbers, and plot these along with the predicted coupling strength:

$$g_n = \boldsymbol{\mu}_m \sqrt{\frac{4\pi\hbar nc}{\lambda\varepsilon\varepsilon_0 V}}$$

where $\boldsymbol{\mu}_m = 3.8D$ is the transition dipole moment of isolated methylene-blue molecules[23]. The probability of finding each coupling strength (Fig. 4a, colour map) follows the Poisson distribution for n molecules under each nanoparticle. The range of Rabi splittings seen for $\bar{n} = 2.5$ that exceed thermal- and cavity-loss rates at room temperature, is consistent with the idea that our plasmonic nanocavity is supporting single-molecule strong coupling. Reassuringly, the range of Rabi frequencies observed increases as the molecular concentration is reduced, as would be expected

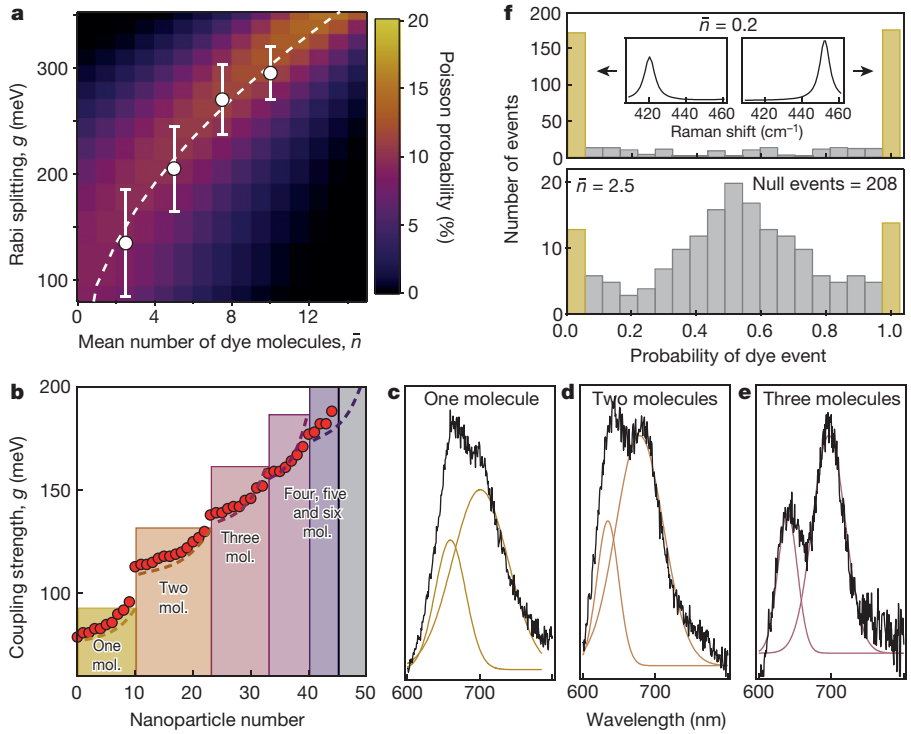

Figure 4 | Rabi splitting from few molecules. a, Energy of Rabi oscillations (g) versus mean number of dye molecules ($\bar{n}$). Experimental (white) points are shown, together with the range of measured coupling strengths (error bars) compared with the theoretical curve (dashed line). The colours represent the Poisson probability distribution of $\bar{n}$. **b**, Coupling strength extracted from different NPoMs in a sample of $\bar{n} = 2.5$. The bars show the theoretical coupling strength obtained from a perfect model; the dashed lines show a random-placement model. **c**–**e**, Scattering spectra for one, two and three molecules (corresponding to **b**), with fits. **f**, Single-molecule probability histograms for $\bar{n} = 0.2$ and 2.5, derived from modified principal-component analysis (Supplementary Fig. 13). The yellow bars show single-molecule events. The insets show the Raman signatures of the two different types of molecular event.

given that $\Delta g(\bar{n}) \propto \sqrt{\bar{n}+\bar{n}^{1/2}} - \sqrt{\bar{n}-\bar{n}^{1/2}}$ similarly increases, as observed in Fig. 4a (colour map).

Direct proof of single-molecule strong coupling is seen from the coupling strengths extracted from the lowest-density samples ($\bar{n} = 2.5$): these show distinct, systematic jumps matching the expected increase in g_n as n rises from one to three dye molecules (Fig. 4b; NPoMs are sorted according to increasing Rabi splitting). The range in each value of g_n arises because single molecules are located at different lateral positions within the gap plasmon, thus coupling with different strengths (predictions are shown as dashed lines in Fig. 4b). Experimentally, we find excellent agreement (with no fitting parameters), showing that a single methylene-blue molecule in our nanocavities gives Rabi splittings of 80–95 meV. Further, we plot the scattering spectrum from $n = 1$–3 molecules, revealing clear increases in coupling strength. Additional proof of the single-molecule strong coupling is seen from the anticrossing of plasmon and exciton modes for the subset with $n = 1$ (Supplementary Fig. 20).

For weakly coupled single molecules, emitted fluorescence should follow the Purcell factor[24–26]. However, such measurements fail here in the strong-coupling regime, because resonantly pumping the molecular absorption also generates strong surface-enhanced resonant Raman scattering (SERRS)—consisting of sharp lines with a strong background—that cannot be uniquely separated from photoluminescence (Supplementary Fig. 11). This also obscures the $g^{(2)}$ measurements that are typically used to confirm single-photon emission from individual chromophores. Here we find extremely strong emission—even though the dye molecules are within 0.5 nm of absorptive gold[27]—owing to the high radiative efficiency of our nanocavities. We harvest these strong SERRS peaks to construct 'chemical' $g^{(2)}_{\mathrm{ch}}$ values, by using the well established bianalyte technique with a second near-identical but distinguishable molecule to prove single-molecule statistics (Fig. 4f and Supplementary Figs 15–17). As clearly evident, at the lowest concentrations two molecules are almost never found at the same time, and we are truly in the single-molecule regime. Although this does not guarantee direct correlation with single-molecule strong-coupling situations, it does prove the statistical probability of single molecules at this concentration. Convincing proof of the presence of single molecules is also provided by the spectral diffusion of vibrational lines in time-series SERRS scans from nanoparticles exhibiting single-molecule strong coupling (Supplementary Figs 18 and 19).

We have succeeded in combining the gap plasmon with oriented host–guest chemistry in aqueous solution to create enormous numbers of strongly coupled, few-molecule nanocavities at room temperature, in ambient conditions, and which are optically addressable. We envisage numerous applications, including single-photon emitters, photon blockades[9], quantum chemistry[28–30], nonlinear optics, and tracked or directed molecular reactions.

Received 16 July 2015; accepted 1 April 2016.
Published online 13 June 2016.

1. Tame, M. S. *et al.* Quantum plasmonics. *Nature Phys.* **9,** 329–340 (2013).
2. Koenderink, A. F., Alù, A. & Polman, A. Nanophotonics: shrinking light-based technology. *Science* **348,** 516–521 (2015).
3. Sato, Y. *et al.* Strong coupling between distant photonic nanocavities and its dynamic control. *Nature Photon.* **6,** 56–61 (2012).
4. Liu, X. *et al.* Strong light–matter coupling in two-dimensional atomic crystals. *Nature Photon.* **9,** 30–34 (2015).
5. Yoshie, T. *et al.* Vacuum Rabi splitting with a single quantum dot in a photonic crystal nanocavity. *Nature* **432,** 200–203 (2004).
6. Thompson, J. D. *et al.* Coupling a single trapped atom to a nanoscale optical cavity. *Science* **340,** 1202–1205 (2013).
7. Faraon, A. *et al.* Coherent generation of non-classical light on a chip via photon-induced tunnelling and blockade. *Nature Phys.* **4,** 859–863 (2008).
8. Gröblacher, S. *et al.* An experimental test of non-local realism. *Nature* **446,** 871–875 (2007).
9. Coles, D. M. *et al.* Strong coupling between chlorosomes of photosynthetic bacteria and a confined optical cavity mode. *Nature Commun.* **5,** 5561 (2014).
10. Shalabney, A. *et al.* Coherent coupling of molecular resonators with a microcavity mode. *Nature Commun.* **6,** 5981 (2015).
11. Törmä, P. & Barnes, W. L. Strong coupling between surface plasmon polaritons and emitters: a review. *Rep. Prog. Phys.* **78,** 013901 (2015).
12. Novotny, L. & Hecht, B. *Principles of Nano-Optics* (Cambridge Univ. Press, 2006).
13. Zengin, G. *et al.* Realizing strong light-matter interactions between single-nanoparticle plasmons and molecular excitons at ambient conditions. *Phys. Rev. Lett.* **114,** 157401 (2015).
14. Zengin, G. *et al.* Approaching the strong coupling limit in single plasmonic nanorods interacting with J-aggregates. *Sci. Rep.* **3,** 3074 (2013).
15. Schlather, A. E., Large, N., Urban, A. S., Nordlander, P. & Halas, N. J. Near-field mediated plexcitonic coupling and giant Rabi splitting in individual metallic dimers. *Nano Lett.* **13,** 3281–3286 (2013).
16. Ciracì, C. *et al.* Probing the ultimate limits of plasmonic enhancement. *Science* **337,** 1072–1074 (2012).
17. de Nijs, B. *et al.* Unfolding the contents of sub-nm plasmonic gaps using normalising plasmon resonance spectroscopy. *Faraday Discuss.* **178,** 185–193 (2015).
18. Benz, F. *et al.* Nanooptics of molecular-shunted plasmonic nanojunctions. *Nano Lett.* **15,** 669–674 (2015).
19. Kasera, S., Herrmann, L. O., del Barrio, J., Baumberg, J. J. & Scherman, O. A. Quantitative multiplexing with nano-self-assemblies in SERS. *Sci. Rep.* **4,** 6785 (2014).
20. Netzer, F. P. & Ramsey, M. G. Structure and orientation of organic molecules on metal surfaces. *Crit. Rev. Solid State Mater. Sci.* **17,** 397–475 (1992).
21. Vahala, K. J. Optical microcavities. *Nature* **424,** 839–846 (2003).
22. Khitrova, G., Gibbs, H. M., Kira, M., Koch, S. W. & Scherer, A. Vacuum Rabi splitting in semiconductors. *Nature Phys.* **2,** 81–90 (2006).
23. Patil, K., Pawar, R. & Talap, P. Self-aggregation of methylene blue in aqueous medium and aqueous solutions of Bu4NBr and urea. *Phys. Chem. Chem. Phys.* **2,** 4313–4317 (2000).
24. Akselrod, G. M. *et al.* Probing the mechanisms of large Purcell enhancement in plasmonic nanoantennas. *Nature Photon.* **8,** 835–840 (2014).
25. Anger, P., Bharadwaj, P. & Novotny, L. Enhancement and quenching of single-molecule fluorescence. *Phys. Rev. Lett.* **96,** 113002 (2006).
26. Kinkhabwala, A. *et al.* Large single-molecule fluorescence enhancements produced by a bowtie nanoantenna. *Nature Photon.* **3,** 654–657 (2009).
27. Kravtsov, V., Berweger, S., Atkin, J. M. & Raschke, M. B. Control of plasmon emission and dynamics at the transition from classical to quantum coupling. *Nano Lett.* **14,** 5270–5275 (2014).
28. Hutchison, J. A., Schwartz, T., Genet, C., Devaux, E. & Ebbesen, T. W. Modifying chemical landscapes by coupling to vacuum fields. *Angew. Chem. Int. Ed.* **51,** 1592–1596 (2012).
29. Galego, J., Garcia-Vidal, F. J. & Feist, J. Cavity-induced modifications of molecular structure in the strong coupling regime. *Phys. Rev. X* **5,** 041022 (2015)
30. Feist, J. & Garcia-Vidal, F. J. Extraordinary exciton conductance induced by strong coupling. *Phys. Rev. Lett.* **114,** 196402 (2015).

Supplementary Information is available in the online version of the paper.

Acknowledgements We acknowledge financial support from the UK's Engineering and Physical Sciences Research Council (grants EP/G060649/1, EP/N020669/1, EP/L027151/1 and EP/l012060/1) and the European Research Council (grant LINASS 320503). This study was partially supported by the Air Force Office of Scientific Research (AFOSR); the European Office of Aerospace Research and Development (EOARD) is also acknowledged. R.C. acknowledges support from the Dr. Manmohan Singh scholarship from St John's College, University of Cambridge. F.B. acknowledges support from the Winton Programme for the Physics of Sustainability. S.J.B. acknowledges support from the European Commission for a Marie Curie Fellowship (NANOSPHERE, 658360).

Author Contributions J.J.B. and R.C. conceived and designed the experiments. R.C. performed the experiments with input from F.B. and B.d.N. R.C. and A.D. carried out the simulation and the analytical modelling with input from J.J.B., P.F., O.H. and E.R. R.C. and J.J.B. analysed the data. S.J.B. and O.A.S. synthesized cucurbit[*n*]uril and provided input on the fabrication and characterization of samples. R.C. and J.J.B. wrote the manuscript with input from all authors.

Author Information Data supporting this paper are available at https://www.repository.cam.ac.uk/handle/1810/254579. Reprints and permissions information is available at www.nature.com/reprints. The authors declare no competing financial interests. Readers are welcome to comment on the online version of the paper. Correspondence and requests for materials should be addressed to J.J.B. (jjb12@cam.ac.uk).